Sensors and Materials, Vol. 37, No. 7 (2025) 2909–2924
MYU Tokyo

S & M 4093

Automated Microcontroller-based Eight-arm Maze for Cognitive Memory Assessment in Rats of Alzheimer's Disease Model

Yu-Rui Hung,[1†] Yu-Lin Wang,[2,3,4†] Shu Cing Wu,[5]
Lung-Chih Kuo,[6] Ching-Ping Chang,[7] and Chi-Chun Chen[8*]

[1]Graduate Institute, Prospective Technology of Electrical Engineering and Computer Science, National Chin-Yi University of Technology, Taichung 411030, Taiwan
[2]School of Medicine, Kaohsiung Medical University, Kaohsiung 807, Taiwan
[3]Department of Biomedical Engineering, National Cheng Kung University, Tainan 701, Taiwan
[4]Department of Physical Medicine and Rehabilitation, Chi Mei Medical Center, Tainan 710, Taiwan
[5]Graduate Institute, Prospective Technology of Electrical Engineering and Computer Science, National Chin-Yi University of Technology, Taichung 411030, Taiwan
[6] Department of Electrical Engineering, National Formosa University, Yunlin 632, Taiwan
[7]Department of Medical Research, Chi Mei Medical Center, Tainan 710, Taiwan
[8]Department of Electronic Engineering, National Chin-Yi University of Technology, Taichung 411030, Taiwan

(Received March 12, 2025; accepted May 23, 2025)

Keywords: automated maze, microcontroller-based maze, radial arm maze, spatial memory, Alzheimer's disease

Alzheimer's disease (AD) is characterized by progressive cognitive decline, with spatial memory impairment being one of its earliest symptoms. To support efficient and accurate behavioral assessments in rodent models of AD, we developed an automated, microcontroller-based radial arm maze integrated with eight infrared (IR) distance sensors. In contrast to traditional camera-based systems, our design eliminates the need for human intervention and visual tracking, offering consistent and reliable performance across diverse lighting conditions. The system enables the precise quantification of latency and short- and long-term memory errors. In validation experiments, rats in the AD group exhibited significantly longer latencies and higher memory error rates than sham controls beginning on Day 21 following Aβ1–42 injection, confirming the system's sensitivity to cognitive decline. Additionally, spatial trajectory maps indicated more disorganized searching patterns and frequent pausing in AD rats. These results demonstrate the effectiveness of the proposed maze system as a robust, low-cost platform for automated cognitive assessment in preclinical AD research.

1. Introduction

Alzheimer's disease (AD) is the most common form of dementia and a leading cause of cognitive impairment in the aging population. One of its earliest clinical features is a progressive decline in spatial memory, which is strongly associated with hippocampal dysfunction.(1,2) To evaluate therapeutic interventions and monitor disease progression, a variety of behavioral

*Corresponding author: e-mail: chichun@ncut.edu.tw
†These authors contributed equally.
https://doi.org/10.18494/SAM5625

ISSN 0914-4935 © MYU K.K.
https://myukk.org/

paradigms have been developed for use in rodent models, including the Morris water maze,[3,4] Y-maze,[5,6] and radial arm maze (RAM).[7,8] Among these, the RAM has received considerable attention for its ability to independently assess both short-term (working) and long-term (reference) memory errors.[9,10]

Traditional implementations of the RAM frequently utilize camera-based tracking systems to monitor rodent behavior.[11,12] Although these systems provide high spatial resolution, they are subject to several critical limitations. First, their performance is highly sensitive to lighting conditions and prone to overexposure—especially on the central platform—resulting in misidentification or data loss.[13,14] Second, image-based systems often misclassify nontarget objects such as droppings or shadows as the animal, leading to erroneous recordings and unnecessarily prolonged trials.[11] These issues necessitate constant human supervision or real-time intervention, thereby reducing experimental efficiency and increasing labor demands. While some research groups have attempted to address these drawbacks using advanced image preprocessing techniques,[15,16] the inherent reliance on stable lighting and controlled environments remains a key constraint. Moreover, recent research has highlighted the need for graphic processing unit (GPU)-intensive computing to support high-resolution tracking, which limits the portability and scalability of such systems for routine behavioral assessments.[17] Collectively, these limitations underscore the need for a reliable, lighting-independent alternative for automated cognitive evaluation in AD models.

To overcome these challenges, the use of IR-sensor-based tracking systems has been investigated in recent research. Unlike vision-based approaches, IR sensors operate independently of ambient lighting and provide high temporal resolution without requiring image processing.[18] These systems also minimize misclassification errors by directly detecting the subject's presence within predefined regions of interest.[19] However, many existing IR-based solutions suffer from limited scalability or involve complex mechanical calibration, which hinders their routine application in behavioral studies.[20] To address these limitations, we propose a novel microcontroller-based radial arm maze equipped with eight IR distance sensors and an automated data acquisition framework. This system is designed to enhance the reliability and efficiency of cognitive assessments in AD rodent models while maintaining high sensitivity to spatial memory performance.

The remainder of this paper is organized as follows. In Sect. 2, we describe the mechanical structure of the automated maze system, along with its hardware and software design. The experimental validation results obtained using Alzheimer's disease (AD) rat models are presented in Sect. 3. In Sect. 4, we provide a detailed discussion of the system's performance, limitations, and potential improvements. In Sect. 5, we conclude the study and include a summary of the findings and suggestions for future research directions.

2. Methods

An automated, microcontroller-based radial arm maze was developed to quantify spatial learning and memory performance in small laboratory animals, such as rats. The apparatus comprises two primary components, namely, a circular central platform and eight detachable arms, all fabricated from black acrylic sheets, as illustrated in Fig. 1. The arms are designed for

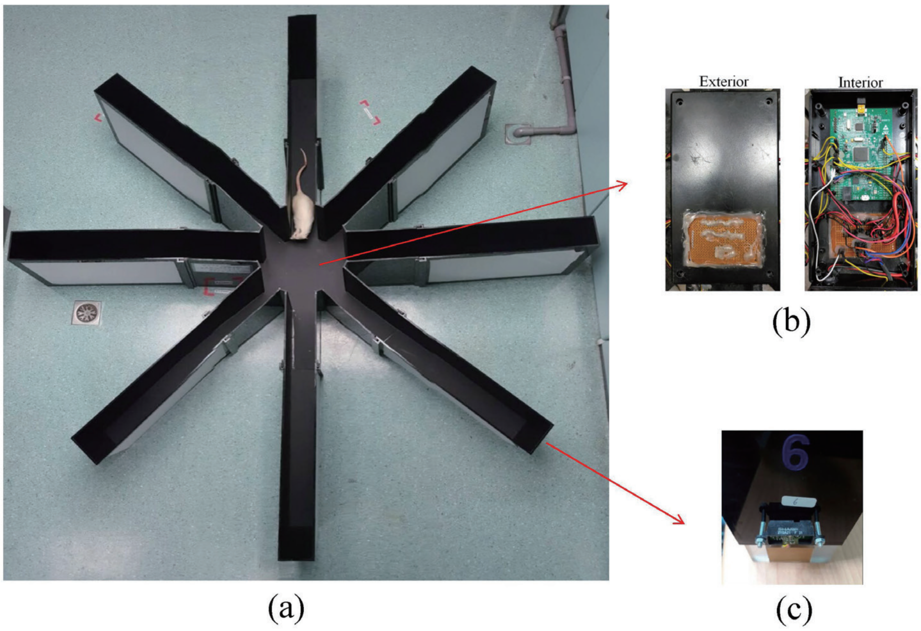

Fig. 1. (Color online) Photographs of the proposed system. (a) Assembled radial arm maze, (b) MCU mounted beneath the central platform, and (c) an IR distance sensor installed at the end of an arm.

plug-in assembly and easy disassembly, allowing for convenient storage and transport. The entire maze is elevated 10 cm above the working surface to accommodate the placement of the microcontroller unit (MCU) and associated electronic components beneath the platform.

A Sharp GP2Y0A21 IR distance sensor is mounted at the end of each arm to detect the presence of the rat. To minimize interference between opposing arms, the sensors are vertically offset at alternating heights of 2 and 3 cm above the maze base. The analog signals from the sensors are collected by an STM32F407 microcontroller, which processes the data to determine the rat's position. The processed data are then transmitted to a PC via a Wi-Fi module (ESP8266), enabling real-time monitoring through a custom graphical user interface. The system supports both local area network (LAN) and Internet-based data communication. During experiments, rats move freely among the arms, and their positional data are continuously recorded for subsequent behavioral analysis.

2.1 Design

Schematics of the maze apparatus are shown in Fig. 2. As illustrated, the central platform has a diameter of 23.5 cm, each arm measures 24.2 cm in length, and the angle between adjacent arms is 45°. A mechanical adaptor measuring $48 \times 10 \times 35$ cm^3 ($L \times W \times H$) connects the arms to the central platform. Each IR sensor is capable of measuring distances up to 80 cm; however, during field tests, interference was observed from opposing sensors owing to overlapping detection zones. To address this signal coupling issue, each opposing sensor pair was mounted at slightly different heights of 2 and 3 cm above the base. This vertical misalignment significantly reduced signal interference, which was further attenuated through digital filtering.

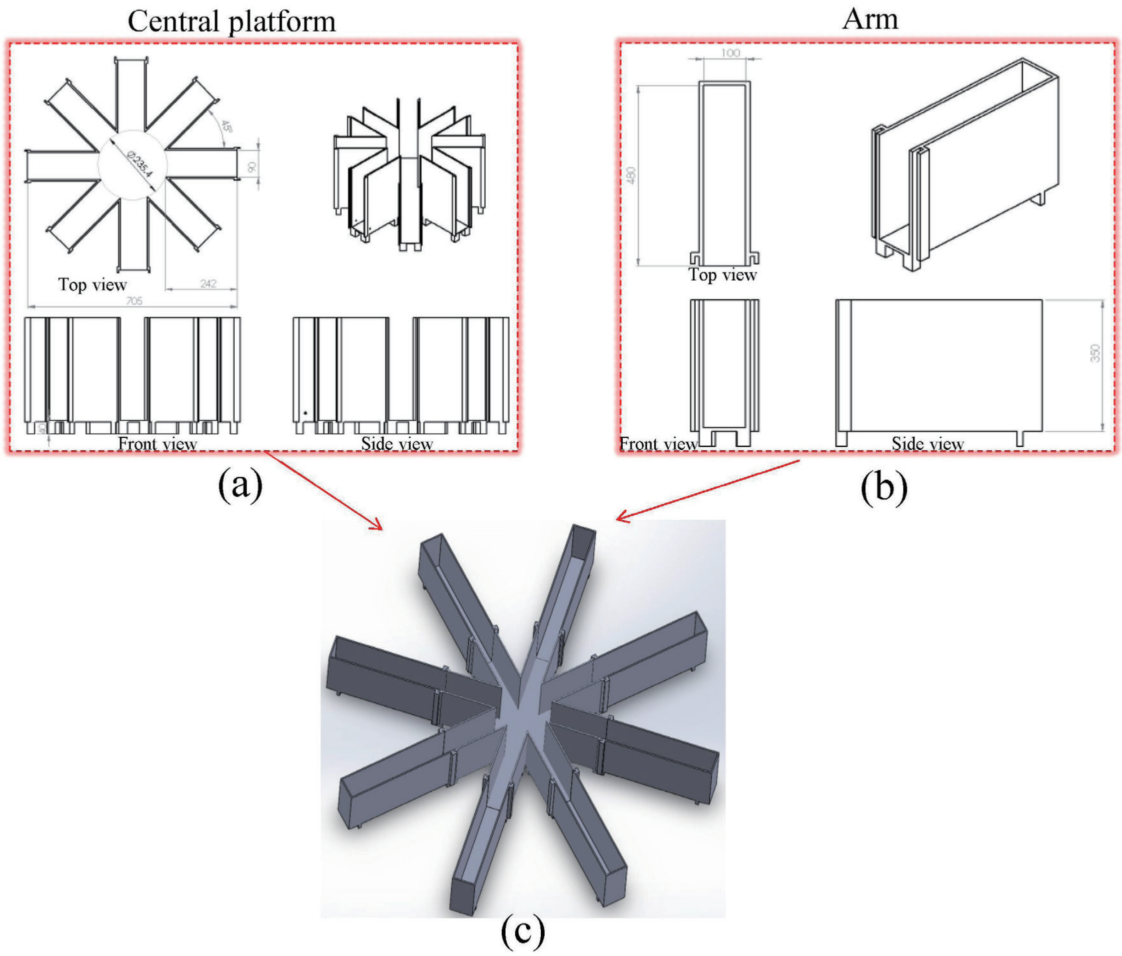

Fig. 2. (Color online) Schematics of (a) the central platform, (b) an arm, and (c) the assembly of (a) and (b).

2.2 Circuits

The subject's position was tracked using eight IR distance sensors connected to an MCU, which transmitted the position data to a PC via a Wi-Fi module. The baited arms were defined through the PC interface prior to each trial. When the rat entered an arm, the corresponding sensor detected its presence, and the system recorded the entry. Conversely, when the rat returned to the central platform, its position was considered invalid and was excluded from arm-specific tracking data.

2.2.1 Control unit

As shown in Fig. 3, the control unit consists of a DC power supply, an STM32F407 microcontroller (STMicroelectronics), eight GP2Y0A21 IR distance sensors, an ESP8266 Wi-Fi module, and a PC. The hardware connections among these components are briefly described below.

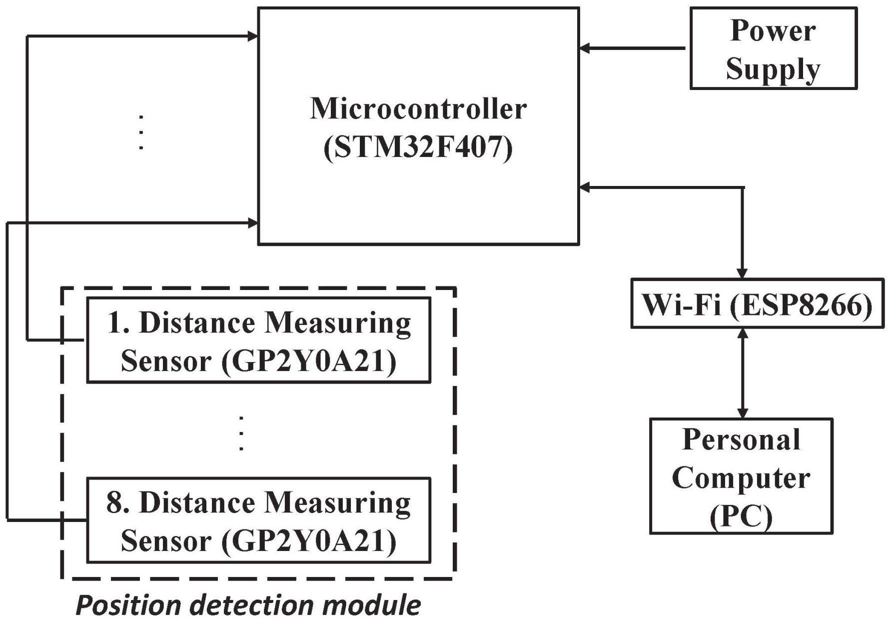

Fig. 3. Hardware links.

2.2.2 Microcontroller

The system is powered by a standard DC power supply, providing stable voltages for both the microcontroller and IR sensors. A high-performance STM32-based microcontroller is responsible for collecting analog signals from the IR sensors, converting them to digital form, and transmitting the processed data to the connected PC via Wi-Fi. This setup enables real-time tracking, error calculation, and latency assessment without the need for manual intervention. The port assignments of the control unit are summarized in Table 1.

2.2.3 IR distance-measuring sensors

In this work, eight Sharp GP2Y0A21 distance-measuring sensors were employed to build the presented maze. Each sensor is an integration of a position-sensitive detector (PSD), an IR emitting diode (IRED), and a signal-processing circuit. The package dimensions are 29.5 × 13 × 13.5 mm^3, providing a distance measuring range of 10–80 cm and an analogue voltage output. In the sensor, the ambient temperature interference can be well reduced by the triangulation method.

2.2.4 Wi-Fi module

ESP8266 is a small-packaged UART Wi-Fi module featuring ultralow power consumption and is exclusively engineered for mobile devices and IoT applications. ESP8266 can be applied to any microcontroller design as a Wi-Fi adaptor through SPI/SDIO or UART interfaces. Physical devices can be connected to IoT or LAN via ESP8266.

Table 1
Microcontroller port assignment.

Port in microcontroller	Function
Port D.12, 13, 14, 15	System status indicator
Port A.1, 2, 3, 4; Port B.1; Port C.5, 13, 14	ADC, capture signal from IR distance sensor
Port B.10, 11	USART, communicate with PC

2.3 Software

Before designing the software, it is important to define the rules defining entry into and exit from the maze arms. Equation (1) represents the distance parameter sensed by any IR sensor over time, where D_{IR_x} represents the sensed distance parameter and x denotes the number of sensors. When a rat enters a particular arm, the corresponding arm sensor starts sensing the distance data between the rat and the end of the arm. A distance of less than 20 cm indicates that the rat has entered that arm, as shown in Eq. (2). Subsequently, the distance of "none" displayed by that sensor signifies that the rat has exited that arm, as depicted in Eq. (3). When Eqs. (2) and (3) occur sequentially, the count of the rat entering that arm once accumulates, as expressed in Eq. (4), where C_{IR_x} represents the cumulative count parameter for that arm.

$$D_{IR_x}(t) = 10 - 80 \text{ cm or none}, \; x = 1, 2, ..., 8 \tag{1}$$

$$D_{IR_x}(t) \le 20 \text{ cm, entering an arm} \tag{2}$$

$$D_{IR_x}(t) = \text{none, exiting an arm} \tag{3}$$

$$C_{IR_x} = C_{IR_x} + 1 \tag{4}$$

The software of the presented radial arm maze system is divided into two parts: (a) firmware loaded in the microcontroller and (b) software loaded in the PC. The former is used to detect the position of the rat in the maze, to evaluate the numbers of long- and short-term memory errors, to evaluate the latency, and to transfer data to the PC, while the latter instructs a user interface and is designed to process and display data.

A firmware, written in C language, was loaded into the microcontroller. It includes a main program and a timer interrupt service routine. As illustrated in Fig. 4(a), the main program receives commands issued by the PC for operation. As the first step, specify four out of the eight arms that contain food at respective food sites. Then, place a rat into the central platform of the maze. The moment the UI button on the PC screen is clicked, maze operation is enabled, and the position of the rat is monitored in real time using the built-in counter in the MCU and eight distance-measuring sensors, and transmitted to the PC for plotting a search pattern over time. As the experiment progresses, the number of times that the rat reaches the end of each arm is

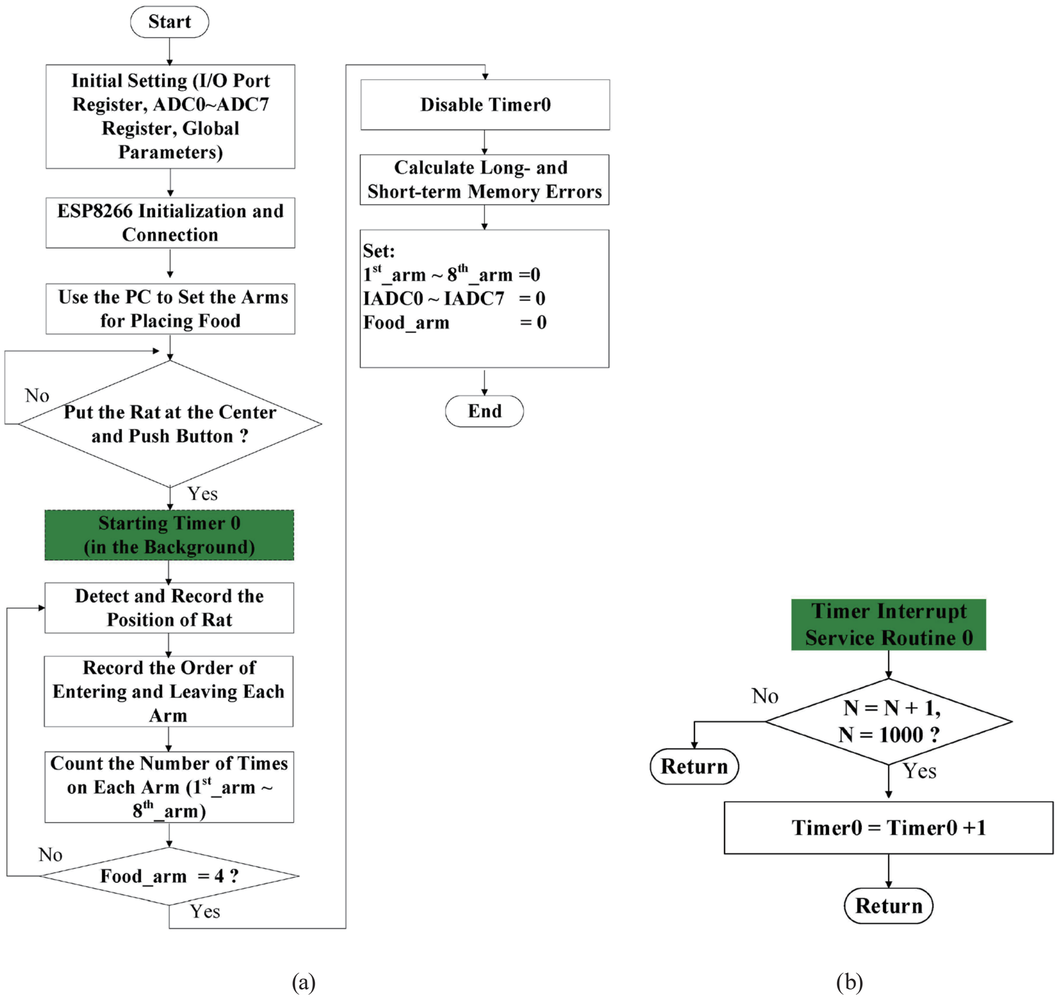

Fig. 4. (Color online) Operation flow chart of (a) the radial arm maze and (b) timer interrupt service routine 0.

counted until the last of the specified arms containing food, and the counter stops instantly. Subsequently, the numbers of long- and short-term memory errors are obtained. As illustrated in Fig. 4(b), Timer Interrupt Service Routine 0 adds 1 to N per millisecond, and then adds 1 to Timer 0 when $N = 1000$, that is, 1 is added to Timer 0 per second.

2.4 Experimental procedures and system validation

Prior to animal testing, system functionality was validated in a darkroom using two object models: a piece of white cardboard and a white stuffed toy, both selected to simulate the body size and reflectance of a laboratory rat. Each object was manually guided from the central platform to the end of each arm to evaluate whether the IR sensors could reliably detect entries within the predefined 10–80 cm sensing range. Across 100 trials, the system achieved an average spatial error of less than 2.5 cm, which is acceptable given that the average rat body length exceeds 20 cm. These trials confirmed the accuracy and responsiveness of the sensor-based tracking under low-light conditions and demonstrated that the system output is not affected by ambient lighting.

Following technical validation, a cohort of male Wistar rats (270–320 g) was obtained from an approved supplier and housed in a controlled environment (24 ± 1 °C, 12 h light/dark cycle) at the Central Animal Facility of Chi Mei Medical Center. All experimental procedures were conducted in compliance with the ARRIVE guidelines and approved by the Institutional Animal Care and Use Committee (IACUC approval number: 108120116). Rats were randomly assigned to either the sham group or the Alzheimer's disease (AD) group. The sham group received intracerebroventricular (ICV) injections of artificial cerebrospinal fluid (aCSF), while the AD group received ICV injections of amyloid beta 1–42 (Aβ1–42) to induce neurodegeneration.

2.4.1 Induction of Alzheimer's disease rat model

Rats were anesthetized using sodium pentobarbital [50 mg/kg, intraperitoneal (i.p.) injection)] (Sigma-Aldrich, St. Louis, MO, USA) and a mixture containing ketamine [4.4 mg/kg, intramuscular (i.m.) injection] (Nankuang Pharmaceutical, Tainan, Taiwan), atropine [0.02633 mg/kg, (i.m.)] (Sintong Chemical, Taoyuan, Taiwan) and rompun [6.77 mg/kg, (i.m.)] (Bayer AG, Leverkusen, Germany). Then, the anesthetized experimental animals were subjected to stereotaxic head positioning and fixed to a Kopf stereotaxic apparatus (STOEITING Co.620, WHEAT LANE WOOD DALE, ILLINOIS 60191/USA). After positioning, the parietal bone of each rat was removed with a drill, and a microinjection syringe [microsyringe with a 28-gauge 3.0-mm-long stainless steel needle (Hamilton)] was implanted on the bregma. The coordinates are 0.8 mm on the vertical axis, 1.4 mm on the horizontal axis, and 4.0 mm in depth. Amyloid beta 1-42 (Aβ1-42) was injected into the bilateral ventricles (lateral ventricles) of the rat using a microdialysis infusion pump (CMA/102; Carnegie Medicine, Stockholm, Sweden) at a rate of 0.7 μl/min, and the overall unilateral volume was 10 μl. After the experimental procedure, the needle was removed, the wound was sutured with 4-0 polyamide suture, and the wound was wiped with iodine. After the operation, the rat was moved to a warm blanket and its body temperature was continuously maintained at 36.5 ºC. The animal was moved to an independent cage only after it was awake, and normal drinking water and feed were maintained.

2.4.2 Maze training and testing protocol

A 7-week program is illustrated in Fig. 5. As can be viewed on the timeline, the program consists of a 2-week training program as the first stage and a 5-week testing program as the second. The day that Aβ injections are performed is treated as a point of reference and denoted as Day 0. Rats were placed into the presented maze and moved of their own free will over the first 2 days of the training stage. Subsequently, food was placed at the food site located at the end of each arm on the first 3–5 days, and the rats were guided to explore the new environment to the end of each arm accordingly. Then, the formal training of 1-week duration commenced on Day −7, so as to make the rats memorize the food locations. The 4-week testing program started on Day 0, and the subjects' performances were assessed on a weekly basis.

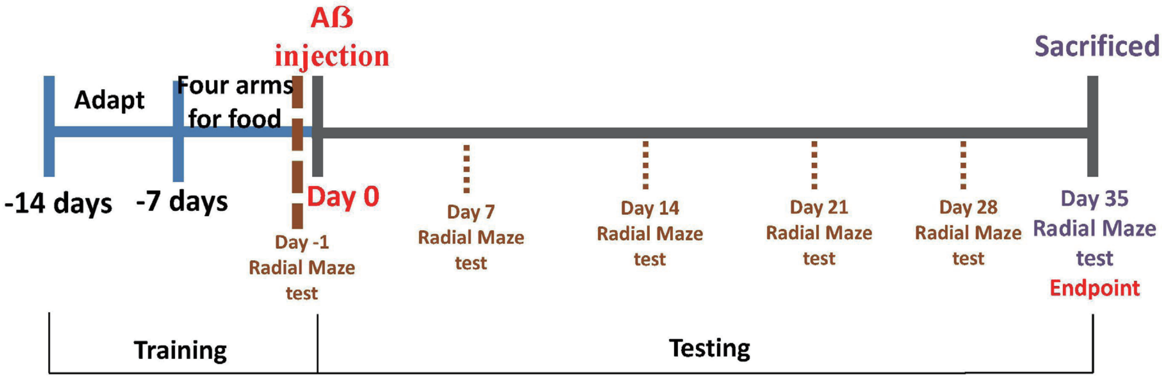

Fig. 5. (Color online) Experimental timeline composed of a 2-week training period and a 4-week testing period with four baited arms.

3. Results

In this study, a computer-side GUI was developed, as shown in Fig. 6. The interface is divided into three sections: the left area for configuration, the central area for the real-time display of the rat's position, and the right area for related quantified cognitive parameters. After selecting the Wi-Fi-associated COM port, researchers can designate the food arms and click the "START" button. The system then automatically begins the detection of the rat's position in the central area while calculating and displaying cognitive parameters in the right area.

Figure 7 illustrates the trajectory maps of AD and sham rats on Day 35, where the rat's position was recorded every 200 ms. If a position point was continuously and repeatedly detected, its area was expanded to represent pausing behavior, with the maximum point diameter reaching 7.92 cm. As shown in Fig. 7, different point diameters correspond to various levels of repeated detections: a 7.92 cm diameter represents more than 2000 consecutive repeated points, a 6.48 cm diameter indicates 1000–1999 points, a 5.04 cm diameter corresponds to 500–999 points, a 4.32 cm diameter represents 200–499 points, a 3.60 cm diameter denotes 100–199 points, a 2.88 cm diameter indicates 10–99 points, and a 0.72 cm diameter represents 1–9 consecutive repeated points. The results clearly showed that the AD rats' trajectories covered almost all eight arms, with numerous large-area position points, indicating frequent pausing behavior. In contrast, the sham rats exhibited fewer pauses, with position points primarily concentrated in the food arms, suggesting preserved spatial memory and goal-directed behavior.

Table 2 shows the distribution of positional trajectories of AD and sham rats at different time points. With time, AD rats exhibited increasingly prominent positional points and pauses. Furthermore, in the later stages, they explored all arms regardless of the presence of food, indicating a progressive decline in spatial memory. In contrast, the sham rats displayed consistent trajectories over a period of weeks, primarily focusing on the arms containing food, with fewer pauses. This behavior suggested that the sham group maintained spatial memory function throughout the experiment.

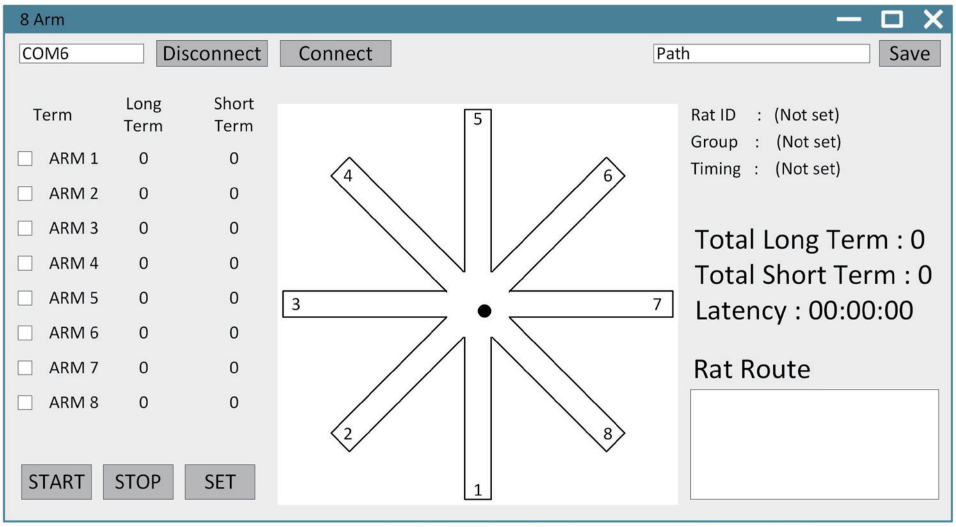

Fig. 6. (Color online) GUI display.

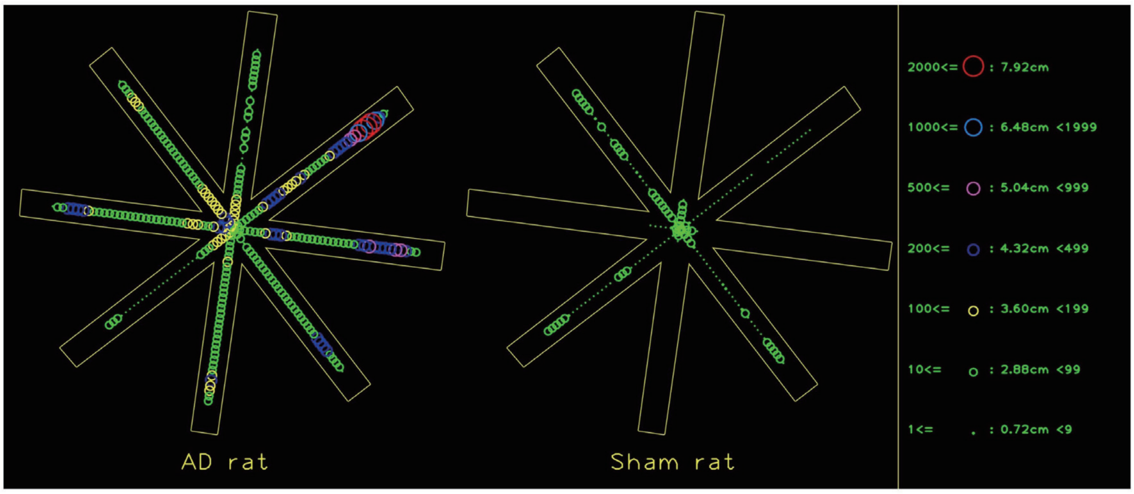

Fig. 7. (Color online) Trajectory maps of AD and sham rats on Day 35.

The spatial memory performance of rodents can be assessed using a radial arm maze. To save manpower and time, an easy-to-use maze apparatus is designed and implemented herein such that the latency and the short- and long-term memory errors can be measured and evaluated automatically. The test performances of the sham and AD groups were compared and discussed as follows.

The average latencies of the sham and AD groups are shown in Fig. 8(a). As can be seen, the sham group had a latency of 400 s or so throughout the 5-week testing program, while the AD group had a latency of 644 s on Day 21, meaning that the spatial memory loss problem developed on Day 21 for the AD group.

The short-term memory errors are shown in Fig. 8(b). There was no statistical difference between the two groups, namely, 4 times for each, until Day 21. However, the AD group showed

Table 2
(Color online) Trajectory presentations of AD and sham rats at different time points.

Days	AD rat	Sham rat
Pre-surgery	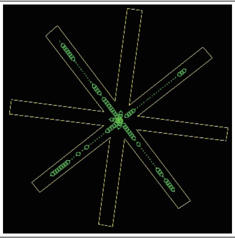	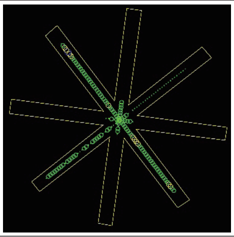
Day 14	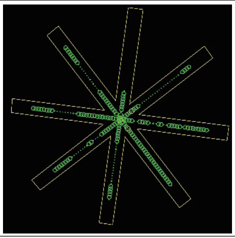	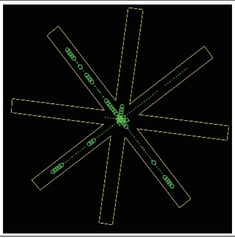
Day 21	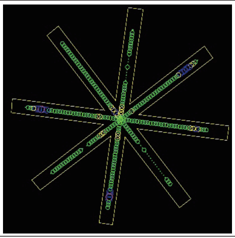	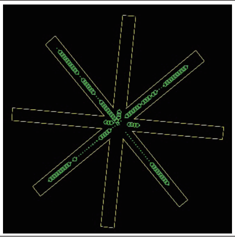
Day 35	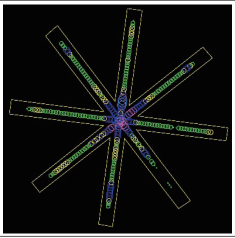	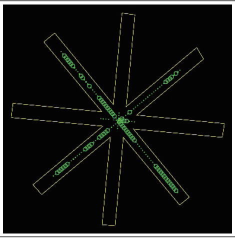

8.9 occurrences of short-term memory error on Day 21. Short-term memory error has been known to appear in the early stage of Alzheimer's disease, that is, Day 21 in this case.

Figure 8(c) shows a plot of long-term memory errors. As it turned out, both groups show error of 2 to 3 times until Day 21. Nonetheless, the upper bound of long-term error, i.e., error of 4 times, was attained on Day 28, meaning that the long-term memory error started to develop from then.

4. Discussion

In this study, we present a user-friendly radial arm maze apparatus specifically developed for the automated assessment of spatial memory performance in experimental subjects. The system integrates a microcontroller and eight IR distance sensors, one mounted at the end of each maze arm. It autonomously records both the timing and frequency of arm entries, thereby enabling the precise evaluation of short- and long-term memory errors. This automated process eliminates the need for manual observation and, more importantly, minimizes the risk of human-induced

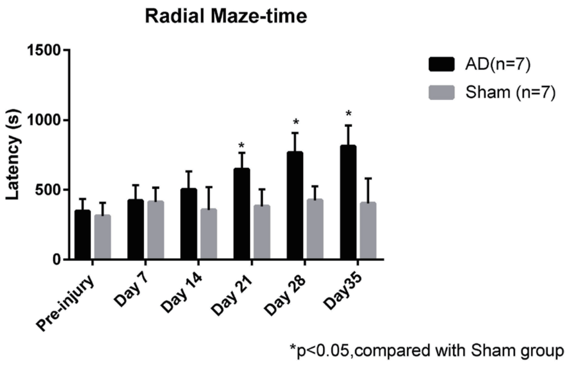

(a)

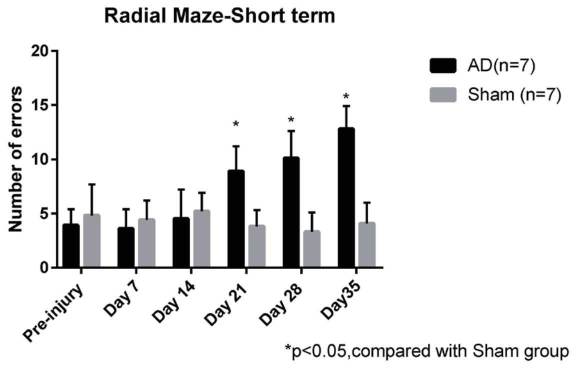

(b)

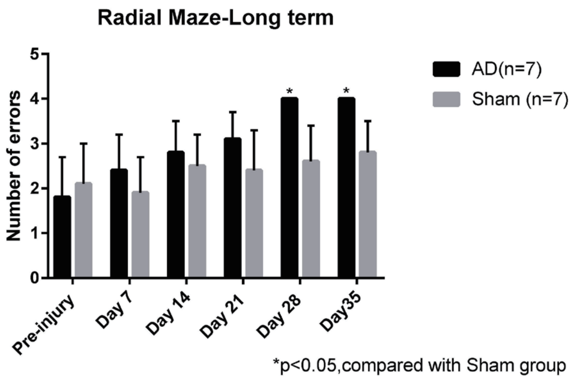

(c)

Fig. 8. Weekly spatial memory performances of sham and AD groups for (a) the latency and (b) short- and (c) long-term memory errors.

errors during data collection. In contrast, most commercial radial arm maze systems rely on image recognition algorithms for subject tracking. However, with those systems, droppings are often misidentified as stationary animals, resulting in prolonged or even indefinite trials, despite the subject's continued exploratory behavior. A frequently adopted but inefficient strategy involves the real-time manual removal of droppings to maintain tracking accuracy. Given that an AD model rat typically requires more than 15 min to complete a food-searching task, researchers are required to monitor the entire trial duration, thereby increasing labor demands considerably. To overcome these limitations, in the present study, an IR-sensor-equipped radial arm maze is introduced as a fully automated and unmanned solution that eliminates tracking-related errors. The system enables the accurate real-time localization of the subject, ensuring the reliable quantification of latency and both short- and long-term memory errors. A key advantage of this design lies in its ability to operate under all lighting conditions, including total darkness, since IR sensors function independently of ambient light.

Table 3 presents the results of a comparative analysis of key features of the proposed IR-sensor-based tracking system and a conventional image-based tracking algorithm [11]. As discussed in Introduction, the proposed method offers improved latency resolution, robust

Table 3
Major features of the two subject tracking techniques.

Features	Image-based tracking algorithm[11]	This proposal
Overlit sensitivity	Susceptible in center area	Not affected (IR is not light dependent)
Latency resolution	~1 s (subject to image processing delay)	0.1 s (sensor polling every 100 ms)
Average position error	~1.2 cm (with post-processing)	~2.5 cm (based on unfiltered raw sensor output)
False detection risk	High (frequent misidentification due to droppings or shadows)	Low (accurate presence detection via direct IR beam interruption)
Computation demand	High (requires GPU acceleration and image preprocessing)	Low (fully executable on a microcontroller)
Lighting condition dependence	High (requires uniform and stable illumination)	None (operates reliably in total darkness)

performance under all lighting conditions, and reduced false detection risk—particularly by eliminating the overexposure and misidentification issues common to camera-based systems. One acknowledged that the limitation of the system is its lower spatial resolution owing to the divergent nature of the IR beam, which precludes the precise localization of the subject within the arm. However, high spatial resolution is not a critical requirement in this context. Unlike applications aimed at analyzing detailed food-searching trajectories, the present study focuses on latency and memory-related metrics, which are independent of fine-grained spatial data. As such, the trade-off in spatial resolution does not compromise the validity or reliability of the cognitive performance assessments provided by the system.

A food-searching task was conducted using the unmanned maze system, while an experimenter simultaneously observed the same trial for validation purposes. The automated tracking results closely matched the direct human observations, demonstrating the accuracy of the system. On rare occasions, the emitted IR beam failed to detect the subject when the rat stood upright and remained motionless, resulting in a temporary absence of signal input. In such cases, the microcontroller interpreted the no-signal condition as the rat pausing on an arm, which accurately corresponded to the animal's actual behavior. This intrinsic alignment between system interpretation and observed behavior further supports the reliability and validity of the proposed tracking method.

A notable feature of the proposed system is its rat-tracking mechanism, which employs eight IR distance sensors, one mounted at the end of each maze arm. While each sensor provides a maximum detection range of 80 cm, field testing revealed signal interference from opposing sensors owing to overlapping detection zones. To address this issue, the sensors were vertically offset—one at 2 cm and the opposing sensor at 3 cm above the maze base—substantially reducing interference. Residual noise was further attenuated by digital signal filtering.

Although this combination of vertical misalignment and digital filtering effectively minimizes signal coupling, it remains a partial solution. To further improve system reliability, future versions will incorporate a sequential time-multiplexed activation strategy, in which only one IR sensor is active at a time within a controlled polling cycle. Such a design eliminates simultaneous IR emissions, thereby preventing cross-talk. The activation sequence will be managed by a timer-interrupt routine on the microcontroller, ensuring the temporal isolation of sensor readings. This enhancement is expected to fully resolve interference issues without compromising detection speed or spatial resolution, ultimately improving system robustness and scalability for broader behavioral research applications.

As noted in previous research,[21] rats instinctively prefer dark, enclosed spaces over brightly lit, open areas. Building on this behavioral principle, we introduce an automated radial arm maze equipped with IR distance-measuring sensors, enabling the reliable cognitive assessment of AD model rats under both dark and illuminated conditions. This feature supports future comparative investigations on how lighting environments affect spatial memory performance. Furthermore, unlike commercial camera-based tracking systems—which are prone to misidentification caused by the presence of shadows or droppings—the proposed IR-sensor-based system avoids such errors entirely, thereby ensuring more consistent and accurate behavioral data.

5. Conclusions

We presented an automated, microcontroller-based radial arm maze designed to assess spatial memory performance in AD rat models. The system employs eight IR distance sensors, one mounted at the end of each arm, to detect subject location. Using position-versus-time data acquired via the microcontroller, latency, and short- and long-term memory errors were quantitatively measured. Experimental results revealed statistically significant differences in all three metrics between the sham and AD groups beginning 21 days after Aβ injection, thereby validating the effectiveness of the proposed system. In addition to its analytical capabilities, the system was developed as a fully unmanned solution to eliminate human observation errors and address the common misidentification issues arising in camera-based tracking systems, such as false detections of shadows or droppings. In conclusion, the proposed maze offers a 100% reliable platform for evaluating spatial memory performance in behavioral experiments, with consistent functionality under all lighting conditions owing to its use of IR-sensor-based tracking.

Acknowledgments

The authors would like to thank Miss Pi-Yu Chao and Miss Jui-Ti Ma from the Department of Medical Research, Chi-Mei Medical Center, No. 901, Zhonghua Rd., Yongkang Dist., Tainan City 701, Taiwan, for their valuable assistance in the experiments with rats.

Data availability

The data that support the findings of this study are available from the corresponding author upon reasonable request.

Competing interests

There is no competing interest.

Authors' contributions

Y-RH, Y-LW, and C-CC established the automatic cognition-assessment-based radial-arm maze system. S-CW, L-CK, and C-PC planned and performed the experiments. Y-RH, Y-LW, and C-CC analyzed the data and conceived and designed the experiments. S-CW, L-CK, and C-PC contributed reagents/materials/analysis tools. C-CC wrote the paper. C-PC designed the animal experiments and statistical analysis.

Ethics approval and consent to participate

The statements on Ethics approval and consent to participate in the study are reported in the Methods–Experimental animals section.

Consent for publication

Not applicable.

Funding

This work was supported by the National Science and Technology Council, Taiwan, under grant number NSTC 113-2221-E-167-006-.

References

1 A. Serrano-Pozo, M. P. Frosch, E. Masliah, and B. T. Hyman: Cold Spring Harbor Perspect. Med. **1** (2011) a006189. https://doi.org/10.1101/cshperspect.a006189
2 J. T. Becker, J. A. Walker, and D. S. Olton: Brain Res. **200** (1980) 307. https://doi.org/10.1016/0006-8993(80)90922-1
3 R. G. M. Morris: Learn. Motiv. **12** (1981) 239. https://doi.org/10.1016/0023-9690(81)90020-5
4 N. Curdt, F. W. Schmitt, C. Bouter, T. Iseni, H. C. Weile, B. Altunok, N. Beindorff, T. A. Bayer, M. B. Cooke, and Y. Bouter: Sci. Rep. **12** (2022) 5451. https://doi.org/10.1038/s41598-022-09270-1
5 C. V. Vorhees and M. T. Williams: ILAR J. **55** (2014) 310. https://doi.org/10.1093/ilar/ilu013
6 A. M. Biomed, G. Revilla, H. Ali, and Almurdi: Iran. J. Med. Sci. **49** (2024) 441. https://doi.org/10.30476/ijms.2023.98912.3104
7 D. S. Olton: Physiol. Behav. **40** (1987) 793. https://doi.org/10.1016/0031-9384(87)90286-1
8 S. C. Wu, C. Y. Lin, L. J. Hong, and C. C. Chen: Sens. Mater. **34** (2022) 2341. https://doi.org/10.18494/sam3725
9 M. F. Brown, R. F. Farley, and E. J. Lorek: J. Exp. Psychol. Anim. Behav. Process. **33** (2007) 213. https://doi.org/10.1037/0097-7403.33.3.213
10 D. Puzzo, L. Lee, A. Palmeri, G. Calabrese, and O. Arancio: Biochem. Pharmacol. **88** (2014) 450. https://doi.org/10.1016/j.bcp.2014.01.011
11 C. C. Chen, L. J. Hong, J. Y. Wang, and C. P. Chang: Sci. Rep. **11** (2021) 22447. https://doi.org/10.1038/s41598-021-01974-0
12 C. D. David, B. N. Wyrosdic, H. Y. Wan, H. E. Lapp, A. A. Bartlett, S. Yitbarek, and J. H. Park: Psychoneuroendocrinology **136** (2022) 105627. https://doi.org/10.1016/j.psyneuen.2021.105627
13 A. Rodriguez, H. Q. Zhang, J. Klaminder, T. Brodin, P. L. Andersson, and M. Andersson: Methods Ecol. Evol. **9** (2018) 460. https://doi.org/10.1111/2041-210x.12874
14 B. Risse, D. Berh, N. Otto, C. Klämbt, and X. Y. Jiang: PLoS Comput. Biol. **13** (2017). https://doi.org/10.1371/journal.pcbi.1005530
15 M. G. Forero, N. C. Hernández, C. M. Morera, L. A. Aguilar, R. Aquino, and L. E. Baquedano: Heliyon **9** (2023) e18367. https://doi.org/10.1016/j.heliyon.2023.e18367

16 P. González-Gaspar, M. Macías-Carballo, T. Cadena-Mejía, M. A. Landa-Jiménez, F. M. Montes-González, M. L. López-Meraz, L. Beltran-Parrazal, and C. Morgado-Valle: Behav. Process. **193** (2021) 104539. https://doi.org/10.1016/j.beproc.2021.104539
17 M. Fernández-Sanjurjo, M. Mucientes, and V. M. Brea: IEEE Internet Things J. **8** (2021) 9177. https://doi.org/10.1109/jiot.2021.3056239
18 Z. X. Liu, M. Yang, Y. Z. Yuan, and K. Y. Chan: IEEE Sens. J. **20** (2020) 9558. https://doi.org/10.1109/jsen.2020.2988070
19 L. L. Yuan, B. Yang, and Q. F. Wei: ISA Trans. **94** (2019) 370. https://doi.org/10.1016/j.isatra.2019.04.022
20 J. Lu, T. Zhang, F. Hu, and Q. Hao: IEEE Trans. Syst. Man. Cybern. **47** (2017) 263. https://doi.org/10.1109/tsmc.2016.2523914
21 C. A. Barnes: J. Comp. Physiol. Psychol. **93** (1979) 74. https://doi.org/10.1037/h0077579